Acta Polytechnica **65**(4):420–428, 2025
https://doi.org/10.14311/AP.2025.65.0420

Published by the Czech Technical University in Prague

LOSS OF PARTICLE RATIO METRIC FOR PARTICLE IMAGE VELOCIMETRY ACCURACY ESTIMATION

Jan Novotný*, Ludmila Nováková, Ilona Machovská, Miloš Kašpárek

Jan Evangelista Purkyně University in Ústí nad Labem, Faculty of Mechanical Engineering, Department of Energy and Electrical Engineering, Pasteurova 3334/7, 400 01 Ústí nad Labem, Czech Republic

* corresponding author: novotny@ujep.cz

Abstract. This paper presents an algorithm for evaluating measurement uncertainty at individual points within the Particle Image Velocimetry (PIV) method. The algorithm presents a novel correlation plane metric known as the Loss of Particle Ratio (LPR). This metric is computed by evaluating the magnitude of two correlation peaks: Mutual Information (MI) and the autocorrelation peak. LPR is defined as the ratio of MI, accounting for the total number of particles contributing to signal peak growth, to the magnitude of the autocorrelation peak, which represents the total number of particles within an interrogation area (IA). The computation of LPR allows both the overall measurement accuracy and the accuracy in each direction to be determined. To improve accuracy, the proposed metric undergoes corrections based on the resultant displacement from the last iteration of the Standard Cross-Correlation (SCC) algorithm and the gradient value within the IA. The process of determining the measurement uncertainty relies on the analysis of synthetic data and the application of two tests – the Uniform Flow Test (UFT) and the Couette Flow Test (CFT). The paper explores the impact of individual corrections on the metric and establishes dependencies between the adjusted metric values and measurement uncertainty. The procedure defines the measurement uncertainty based on synthetic test parameterisation, considering key parameters that influence accuracy, such as the density of particles within the IA, the velocity gradient, the particle diameter, the displacement in the last iteration, and the noise level. The synthetic test parametrisation employs various methods for defining the gradient within the IA. The proposed procedure for determining the measurement uncertainty, utilising the corrected metric Loss of Particle Ratio, is compared with an approach based on synthetic test parameterisation for the Standard Cross-Correlation algorithm. The study contributes insights into the effectiveness of the proposed algorithm in assessing measurement uncertainty, offering a comprehensive comparison with existing methodologies.

Keywords: Particle image velocimetry, accuracy, metric, synthetic tests, uncertainty.

1. Introduction

Since the introduction of the Particle Image Velocimetry (PIV) measurement method, researchers have sought to evaluate the magnitude of measurement uncertainty. However, in the mid-1980s, the PIV measurement system differed significantly from its contemporary counterpart. Continuous lasers were predominantly used in lieu of pulsed lasers, and traditional cameras equipped with sensitive films were used for detecting the movement of seeding particles. Determining the displacement of particle images primarily relied on optic Fourier transformation, followed by digitisation. Despite the initial complexity and duration of determining the particle image displacement in the early stages of the PIV measurement method, [1] presented a study addressing the probability of signal peak detection. This study examined the correlation between the probability of detecting signal peaks and a parameter defined as "Effective particle density". In the following years, this procedure was complemented by standardised synthetic tests [2–6]. In these articles, the authors compare individual algorithms and their sensitivity to the quality of the recorded image. For more than twenty years since the PIV method was established, these two approaches were the only possibility of how to compare the accuracy of individual algorithms and how to estimate the measurement accuracy. A detailed analysis of determining the measurement accuracy is provided by [6, 7], giving a very detailed overview of existing methods and procedures for determining the accuracy of PIV measurements. A comparative assessment of the PIV uncertainty quantification (PIV-UQ) methods written by [8] gives an overview of four recently proposed methods – the uncertainty surface method [5], the particle disparity approach [9], the peak ratio criterion [6], and the correlation statistic method [10]. Boomsma et al. [11] also deal with the comparative experimental evaluation of uncertainty quantification methods, illustrating strengths and weaknesses of the methods and identifying future directions for further development and improvement.

In 2013, Xue et al. [12] published a new procedure for determining measurement uncertainty based on defining a suitable metric of the correlation plane and determining relationship between the metric value and

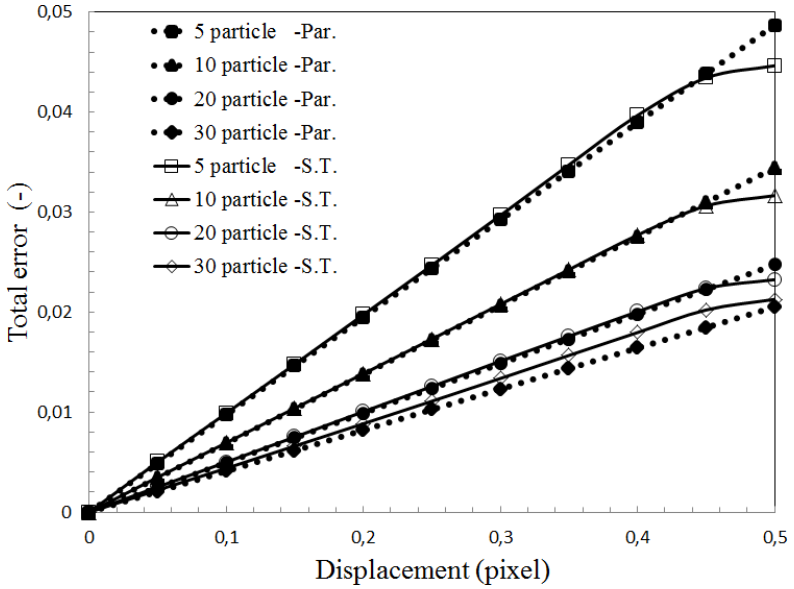

FIGURE 1. Influence of density on the magnitude of particle displacement. Comparison of results of synthetic tests (S.T.) and the discovered parametric dependence (Par.).

the measurement uncertainty based on an analysis of synthetic tests, such as the Uniform Flow Test and the Couette Flow Test. In the following years, Xue [13] expanded this theory by using a new metric referred to as Mutual Information, which allowed for a more accurate determination of the correlation between the metric value and the measurement uncertainty. A real flow-field application of uncertainty estimation using the MI metric was presented by Xue [14]. Recently, other authors dealing with the issue of accuracy in PIV measurement have been focusing on the issue of micro PIV particle tracking velocimetry and the use of neural networks [15–17]. Novotny et al. [18, 19] published the possibility of using corrected metrics to accurately determine the correlation between the metric values and the measurement error. In our work, we aim to build on the findings of authors Xue et al. [13] and define a new metric based on the principle of determination of the MI value. Another aim of this work is to find a link between the results of synthetic tests and the metric of the correlation plane. This work builds on and extends the collective's original work [20] on this topic presented at the 2018 conference.

2. Parameterisation of main characteristics

The results of synthetic tests for the SCC algorithm are well known and have been published many times. The total measurement error in pixels is primarily influenced by the following parameters:

- The size of the particle image is characterised by the diameter of the detected particles in pixels.
- Particle density is quantified as the count of individual particles within a specified Interrogation Area (IA).
- Displacement magnitude is measured as the relative particle displacement in pixels, highlighting both the total displacement magnitude and the displacement determined in the last iteration.
- IA size is established by the dimensions of the edge of the interrogation area in pixels.
- The magnitude of the velocity gradient is computed as the disparity in displacement on opposite sides of the IA divided by the diameter of the seeding particle.
- The noise level is determined under the assumption of symmetrical noise distribution, ascertained through the detection of the histogram peak in recorded images [21].

A specific objective of this work is to develop a set of equations that describe the results of synthetic tests for the SCC method as a function of key parameters. Another objective is to estimate the total measurement error using these parametric equations. All of the equations presented in this work are the result of optimisation analyses applied to the synthetic test data. Figure 1 shows a comparison of the results of the Uniform Flow Test, Total error depending on the displacement, and a suitable parametric equation (in pixels). The equation describing the UFT results according to Figure 1 can be written, for both directions, as follows:

$$\begin{aligned} \delta_{dx,\mathrm{Ni}} &= dx \cdot \left(0.16 \cdot \mathrm{Ni}^{-0.42} + \frac{0.08}{\mathrm{Ni}}\right), \\ \delta_{dy,\mathrm{Ni}} &= dy \cdot \left(0.16 \cdot \mathrm{Ni}^{-0.42} + \frac{0.08}{\mathrm{Ni}}\right), \end{aligned} \tag{1}$$

where Ni is the density of the seeding particles in an area of 32×32 pixels, dx and dy are the subpixel values of the displacement detected in the last iteration.

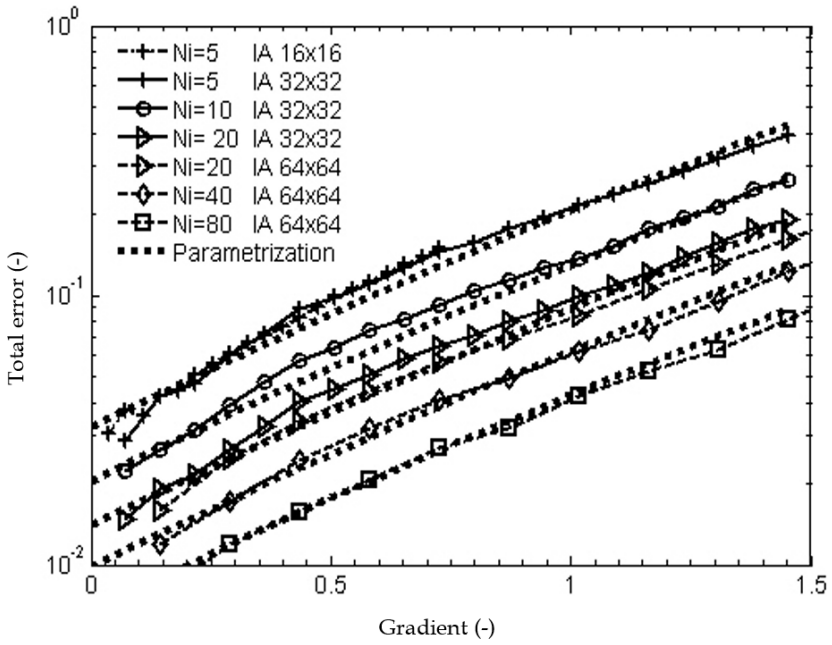

Figure 2. Influence of density on the velocity gradient. Comparison of the results of synthetic tests for different IA and seeding density Ni and discovered parametric dependence.

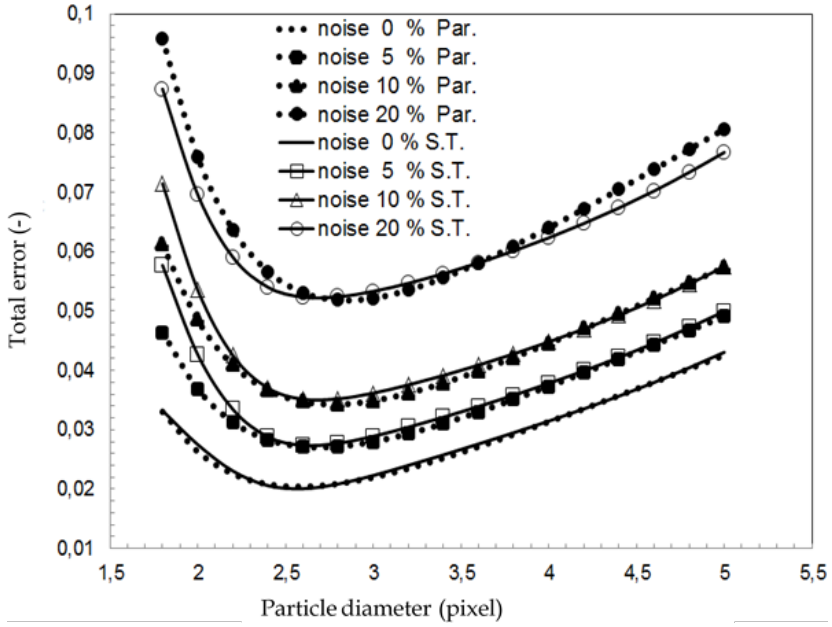

Figure 3. Influence of particle size on total error for noise level Ni = 20, $dx = 0.5$ pixel. Comparison of the results of synthetic tests (S.T.) and the discovered parametric dependence (Par.).

The constants 0.16, −0.42 and 0.08 are the result of optimisation analyses associated with the fitting. The dependence of the total measurement error on the velocity gradient level is usually determined with the help of the Couette Flow Test and is shown in Figure 2. In this diagram, the gradient value is a function of the diameter of the seeding particles, in contrast to the conventional size of the edge of the IA. The reason for using this gradient definition, defined by [1], is that with such a defined gradient, the resultant CFT dependencies form a mutually displaced set of curves suitable for parameterisation, as shown in Figure 2.

The set of equations describing the CFT results depending on the main parameters can be written as:

$$\delta_{\mathrm{Gr}} = 0.7 \cdot K_{\mathrm{Ni}}\left(\left(0.015 \cdot e^{1.6 \cdot \mathrm{Gr}}\right) + 0.02 \cdot \mathrm{Gr}\right), \quad (2)$$

$$K_{\mathrm{Ni}} = 5.77 \cdot N_i^{\left(-\frac{4}{7}\right)}, \quad (3)$$

where KNi is the particle density coefficient and Gr is the gradient value. All constants in Equations (2) and (3) are the result of optimisation analyses associated with the fitting.

Other parameters that affect the total measurement error are the particle image size and noise level. Figure 3 shows the results of the corresponding synthetic

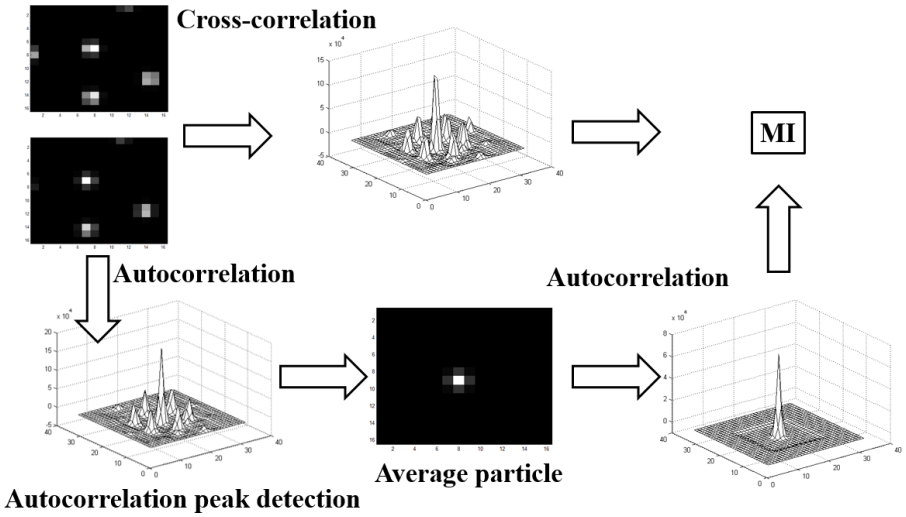

FIGURE 4. Schematic illustration of procedure for calculating MI.

tests for the UFT. This diagram shows the dependence of the total error on the noise level for particle density Ni = 20 and for a single displacement of 0.5 pixels.

The parametric set of equations describing the UFT results shown in Figure 3 can be written as:

$$\delta_{\mathrm{No},dp} = K_{\mathrm{No}} \cdot \left(e^{-2 \cdot dp} + \frac{dp \cdot 1.15 - 1.5}{100} \right) - (dp - 2.6) \cdot \frac{\mathrm{No}}{16}, \tag{4}$$

$$K_{\mathrm{No}} = \left(9 \cdot N_o^{+} 6.2\right) \cdot N_o + 1, \tag{5}$$

where dp is the particle diameter in pixels, K_{No} is the noise level coefficient and No is the noise level. The noise level No was determined from the histogram for each IA separately [22].

The error determined using the approximation (4) assumes a maximum possible displacement measured in the last iteration, i.e. 0.5 pixels and particle density Ni = 20. Since the influence of both the noise level and the particle diameter is dependent on the density and displacement of particles within the IA, the coefficient $\delta_{\mathrm{No},dp}$, calculated according to the Equation (4), has to be modified by coefficients $K_{dx,\mathrm{Ni}}$ and $K_{dy,\mathrm{Ni}}$. Coefficient $K_{dx(dy),\mathrm{Ni}}$ is defined by the following equation:

$$K_{dx,\mathrm{Ni}} = \frac{\delta_{dx,\mathrm{Ni}}}{\delta_{dx=0.5,\mathrm{Ni}=20}}, \qquad K_{dy,\mathrm{Ni}} = \frac{\delta_{dy,\mathrm{Ni}}}{\delta_{dy=0.5,\mathrm{Ni}=20}}. \tag{6}$$

After the specification of all the necessary parameters and determining the total error using the approximated relations, the final equation by means of which the overall measurement accuracy can be determined at a given point and direction can be written as:

$$\delta_{\mathrm{total},dx} = \sqrt{\delta_{\mathrm{Gr}}^2 + K_{dx,\mathrm{Ni}}^2 \delta_{\mathrm{No},dp}^2}, \qquad \delta_{\mathrm{total},dy} = \sqrt{\delta_{\mathrm{Gr}}^2 + K_{dy,\mathrm{Ni}}^2 \delta_{\mathrm{No},dp}^2}. \tag{7}$$

The total measurement error is then given by the equation:

$$\delta_{\mathrm{total}} = \sqrt{\delta_{\mathrm{total},dx}^2 + \delta_{\mathrm{total},dy}^2}. \tag{8}$$

Equations (7) and (8), with the knowledge of all the main parameters defining the features of the recorded data, allow the user to determine both the total measurement error at each point in the measured area, as well as the measurement error in the x-axis and y-axis directions.

3. Correlation plane metrics

The definition of a suitable metric within the correlation plane was described in detail by [12, 13]. This work defines metrics, such as the Primary Peak Ratio PPR and Mutual Information MI.

The metric value MI, according to the calculation given by [11] and as shown in Figure 4, can be interpreted as a number of particles actively involved in the signal peak growth. The MI calculation is based on determining the image of the "average" particle within each IA and the subsequent calculation of the autocorrelation peak. The diameter of this particle is defined by the diameter of the autocorrelation peak IA and the height of the peak is given by the maximum value inside the IA. The MI value is given by the ratio of the size of the signal peak to that of the autocorrelation peak, which is generated by the average particle. Although this method of defining the metric is a breakthrough – it is an easy and robust procedure for determining the number of particles actively contributing to the signal peak growth, and thus to the improvement of the signal-to-noise ratio, it still has a few shortcomings. The value of the determined metric does not take into account the total number of particles in the area or the number of lost pairs. The results of the synthetic tests also show a significant impact of the detected

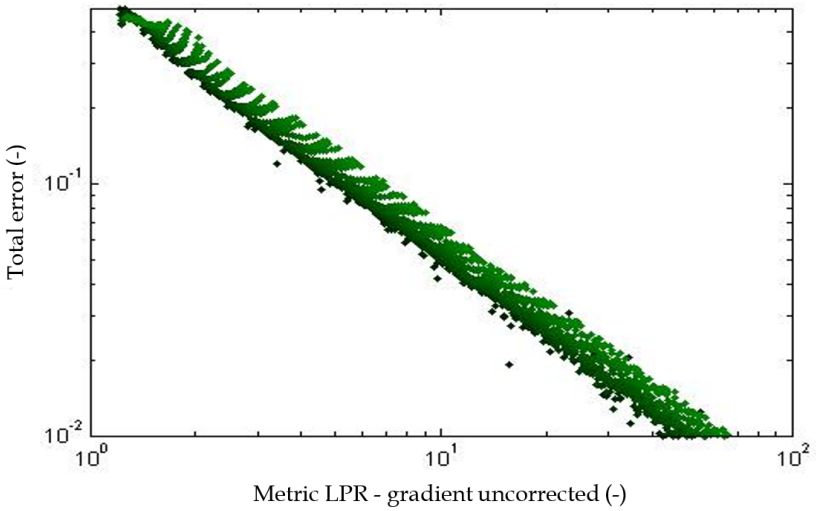

FIGURE 5. Relationship between the LPR metric and the total error. The result of synthetic test – CFT for gradient in the range Gr = 0–1.5 and Ni = 5–30.

displacement in the last iteration and of the gradient level. For these reasons, we proposed correcting the MI metric by the value of the total number of particles within the IA. According to Figure 4, a calculation of Ni can be achieved by a simple correction to the algorithm used to calculate the MI value as suggested by [11]. The only difference between the Ni and MI calculations is that, rather than determining the ratio of the Cross-Correlation peak magnitude and the average particle peak, the ratio is calculated as a ratio of the autocorrelation peak magnitude to the average particle peak. A new metric is suggested that will take into account both the total number of particles and the number of particles contributing to the signal peak growth is suggested. It is written as follows:

$$\mathrm{LPR}_{\mathrm{MI},dx,\mathrm{Ni}} = \mathrm{MI} \cdot (0.01 + 2 \cdot d_x \cdot N_i)^{-1} \quad (9)$$

This metric is labelled as Loss of Particle Ratio and is corrected by the maximum value of the displacement detected in the last iteration. For such a defined metric, the correlation between the metric value and the measurement error according to Figure 5 can be determined with the help of synthetic tests. In our case, we employed a classic multi-step standard correlation algorithm with an IA size of 32×32 pixels. The particle density was modelled in the range from 5 to 30 particles. The particles were always considered to be circular with a Gaussian signal without an average scattering. Images with a particle diameter of 2.2, 3, and 4 pixels were tested. With respect to the particle diameter, the gradient in the test data for the CFT test was considered to be in the range from 0 to 1.5. As shown in Figure 5, the use of the LPR metric also allows us to determine the suitable mathematical correlation between the metric value and the measurement error. The dispersion of values, indicated by the metric, is due to a different levels of the tested gradient. Since the proposed metric is corrected only by the displacement value, it is possible to correct the resultant metric using the gradient value as shown in the following equation:

$$\begin{aligned}\mathrm{LPR}_{\mathrm{MI,Gr},dx,\mathrm{Ni}} = &(\mathrm{MI} \cdot (1 - 0.4 \cdot \mathrm{Gr})) \\ &\cdot (0.01 + 2 \cdot d_x \cdot N_i)^{-1}\end{aligned} \quad (10)$$

The correction of the metric by the LPR gradient, as shown in Figure 6, minimises the dispersion caused by the gradient and a correlation between the value of the corrected metric and the total measurement error can clearly be seen. Although using the corrected metrics according to the Equation (10) clearly yields better results, it is still possible to see a certain variance of values in Figure 7. This variance is particularly noticeable for metric values close to the minimum value of 1 and for metric values greater than 10 (see Figure 6 for details). This variance in values can be eliminated by correcting the MI algorithm. In the results presented by us, the MI is calculated according to the algorithm shown in Figure 4. In this algorithm, the MI value is determined as the maximum size of the correlation peak. However, this value varies depending on the size of the particle displacement and can be up to 50 % lower than the correct value. In order to eliminate this distortion, the correct value of the maximum in the correlation plane must be determined either through point regression or by employing a three-point subpixel interpolation according to the following equation:

$$I_x = \frac{R(x,y)}{\exp\left(\frac{-(x-x_0)^2}{\frac{D_x^2}{8}}\right)}, \quad (11)$$

where $R(x,y)$ is the value in the centre of the correlation peak, x_0 is the true position of the peak in the correlation plane, D_x and D_y (assuming a Gaussian

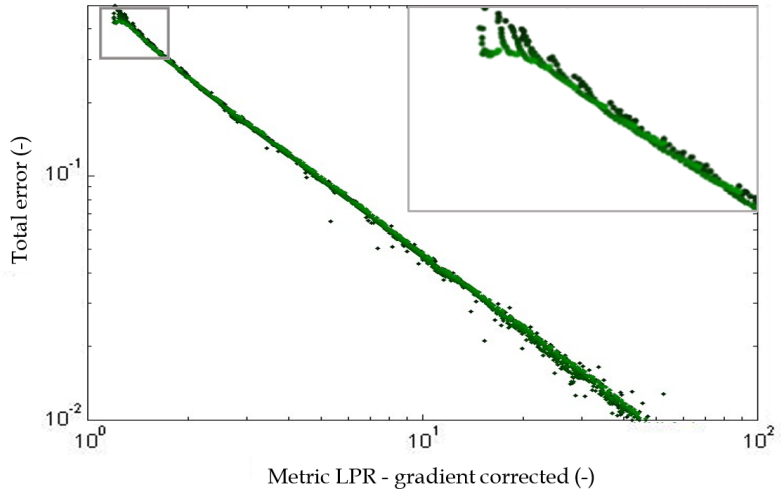

FIGURE 6. Relationship between the gradient-corrected LPR metric and total error. The result of synthetic test – CFT for gradient in the range Gr = 0–1.5 and Ni = 5–30. A detail of the metric values between 0 and 2 is in the upper right corner.

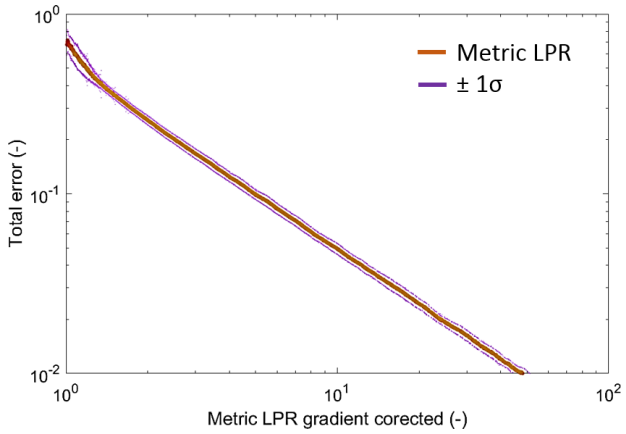

(A). Dependence of the total error determined on the basis of a fully corrected LPR metric and the corresponding range of the standard deviation 1σ.

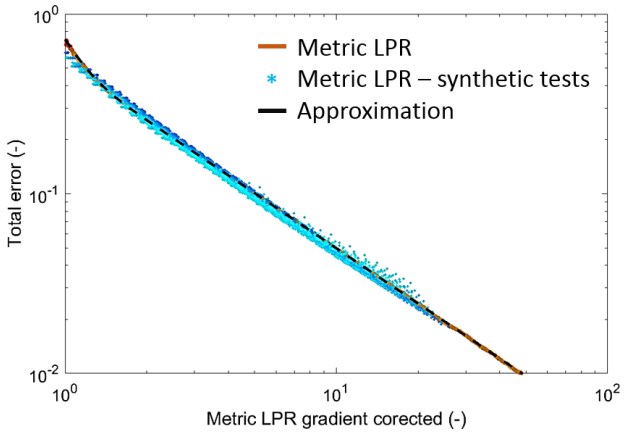

(B). Resultant comparison of the LPR metric and the functional dependence found between the metric value and the measurement error.

FIGURE 7. Comparison of the gradient-corrected LPR metric and LPR calculated from synthetic test. The result of synthetic test – CFT for gradient in the range Gr = 0–1.5, Ni = 5–30, and dp = 2–4.5.

particle shape) are the diameters of the peak in directions x a y, respectively, and are calculated according to the following equation:

$$D_x = \sqrt{\frac{32(x - x_0)}{\ln(R(x-1,y)) - \ln(R(x+1,y))}}. \quad (12)$$

The resulting comparison using a more accurate determination of the peak maximum in the correlation plane is shown in Figure 7. Figure 7a shows the dependence of the total error determined on the basis of a fully corrected LPR metric and the corresponding range of the standard deviation 1σ. It is obvious that the value of 1σ is constant in the whole range of the tested values at the level of about 6 % of the determined value of the total error. The only exception is the area in whichh the LPR metric values are less than 1.4. In this area, the value of 1σ is more than doubled and corresponds to about 14 % of the total error. The aim of this study was not only to determine a suitable metric defined from the correlation plane but also to find a link between the results of the synthetic tests and their parameterisation and the correlation plane metrics. Assuming our predictions are correct, such a metric can be defined as a function of the main parameters that will display the same functional dependence between the metric value and the measurement error as the corrected LPR metric. An equivalent metric defined by the main parameters affecting the quality of the correlation plane can be written as:

$$\begin{aligned} \mathrm{LPR}_{\mathrm{Ni,Gr},dx,dp} &= 0.25 + \left(N_i^{\frac{4}{7}} \cdot (1 - 0.44 \cdot \mathrm{Gr})\right) \\ &\quad \cdot \left(0.16 + 0.2 \cdot dx + \frac{dp}{200} + 0.44 \cdot \mathrm{Gr}\right)^{-1}, \\ \mathrm{LPR}_{\mathrm{Ni,Gr},dy,dp} &= 0.25 + \left(N_i^{\frac{4}{7}} \cdot (1 - 0.44 \cdot \mathrm{Gr})\right) \\ &\quad \cdot \left(0.16 + 0.2 \cdot dy + \frac{dp}{200} + 0.44 \cdot \mathrm{Gr}\right)^{-1}, \end{aligned} \quad (13)$$

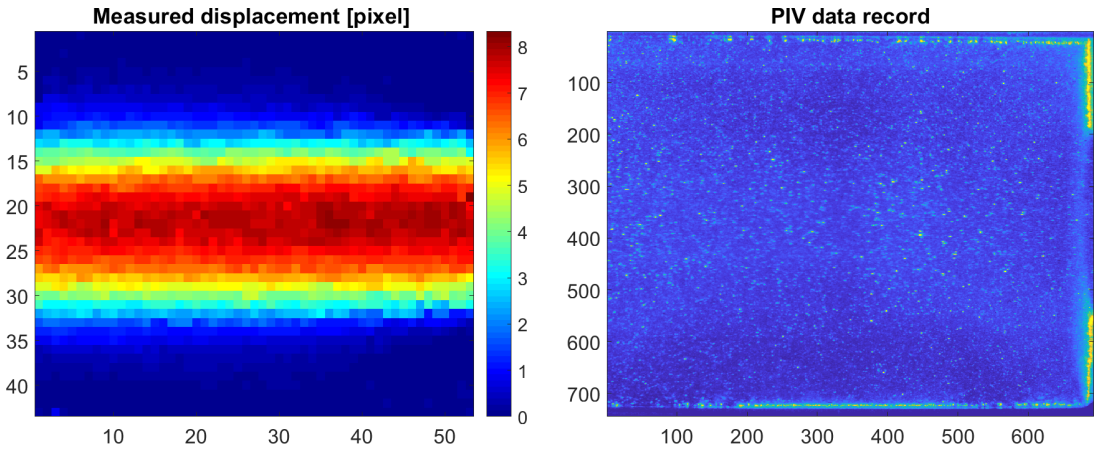

(A). Image recorded by CMOS time-resolved camera.

(B). Evaluation of displacement in pixels.

FIGURE 8. 2D PIV measurement of sudden expansion. Circular pipe, extension ratio of 1:2.

$$\mathrm{PR} = \sqrt{\mathrm{LPR}_{\mathrm{Ni,Gr},dx,dp}{}^2 + \mathrm{LPR}_{\mathrm{Ni,Gr},dy,dp}{}^2}. \quad (14)$$

Figure 7b shows the resultant comparison of both metrics and the functional dependence found between the metric value and the measurement error. The equation describing the correlation can be written in the form suggested by [11]:

$$\sigma^2 = \left[17.55 \cdot e\left[-0.32\left[\frac{\mathrm{LPR}}{0.18}\right]^2\right]\right]^2 + \left(0.52 \cdot \mathrm{LPR}^{-1.02}\right)^2 + (0.001)^2. \quad (15)$$

The equivalent equation to determine the measurement error depending on the MI metric, in the form given by [11], is given by the following relation:

$$\sigma^2 = \left[26.22 \cdot e\left[-0.5\left[\frac{\mathrm{MI}}{2.144}\right]^2\right]\right]^2 + \left(0.8739 \cdot \mathrm{MI}^{-0.9439}\right)^2 + (0.05)^2. \quad (16)$$

In Equations (15) and (16), the constants listed at the end of the equation are threshold values defining the minimum measurement error. All other constants in these equations are the result of optimisation analyses associated with the fitting.

4. Case study: Symmetric flow with sudden expansion

In order to compare the MI metric, as defined in [11], with the LPR metric, we selected a symmetric flow in a circular channel with a sudden expansion (Figure 8). The maximum displacement value in the middle of the measured area was approximately 8.5 pixels, while the minimum approached zero. The number of particles within the area of 32×32 pixels ranged from 4 to 15 particles.

The comparison clearly shows that, for larger values of the measured displacement, both approaches give very similar results. The main difference is in determining the accuracy of the measurement in areas in which the measured displacement approaches zero. In these areas, the measurement error determined on the basis of the MI value is several times greater than the measured displacement and, in principle, is proportional only to the number of particles in the area. For this reason, in places with an offset of less than one pixel, the resulting accuracy determined according to the MI metric does not reflect the effect of the magnitude of the offset measured in the last iteration. Our LPR metric, which corrects the MI value by the number of Ni particles and the gradient, tries to eliminate this shortcoming. Another parameter that affects the size of the LPR metric is the measured offset in the last step of the iteration algorithm. The resulting comparison is shown in Figure 9.

5. Conclusion

Based on the knowledge of synthetic test, we have found a suitable set of equations to describe the UFT and CFT results for the SCC algorithm. We also defined a new metric – the Loss of Particle Ratio, which suitably describes the quality of the flow field. The LPR metric is defined as a corrected ratio of the number of seeding particles contributing to the correlation plane growth and the total number of particles within the IA. We proposed correcting the LPR metric by using the magnitude of the displacement detected in the last iteration and the gradient value within the IA. We also designed and tested the use of the LPR metric, which is based on knowledge of the main parameters that define the quality of the recorded image. Both metrics were compared and a common dependence for the determination of the measurement error was found.

Although the use of the LPR matrix appears suitable for determining the total measurement error, in the following work, it is necessary to clarify the influence of several parameters that were not considered in

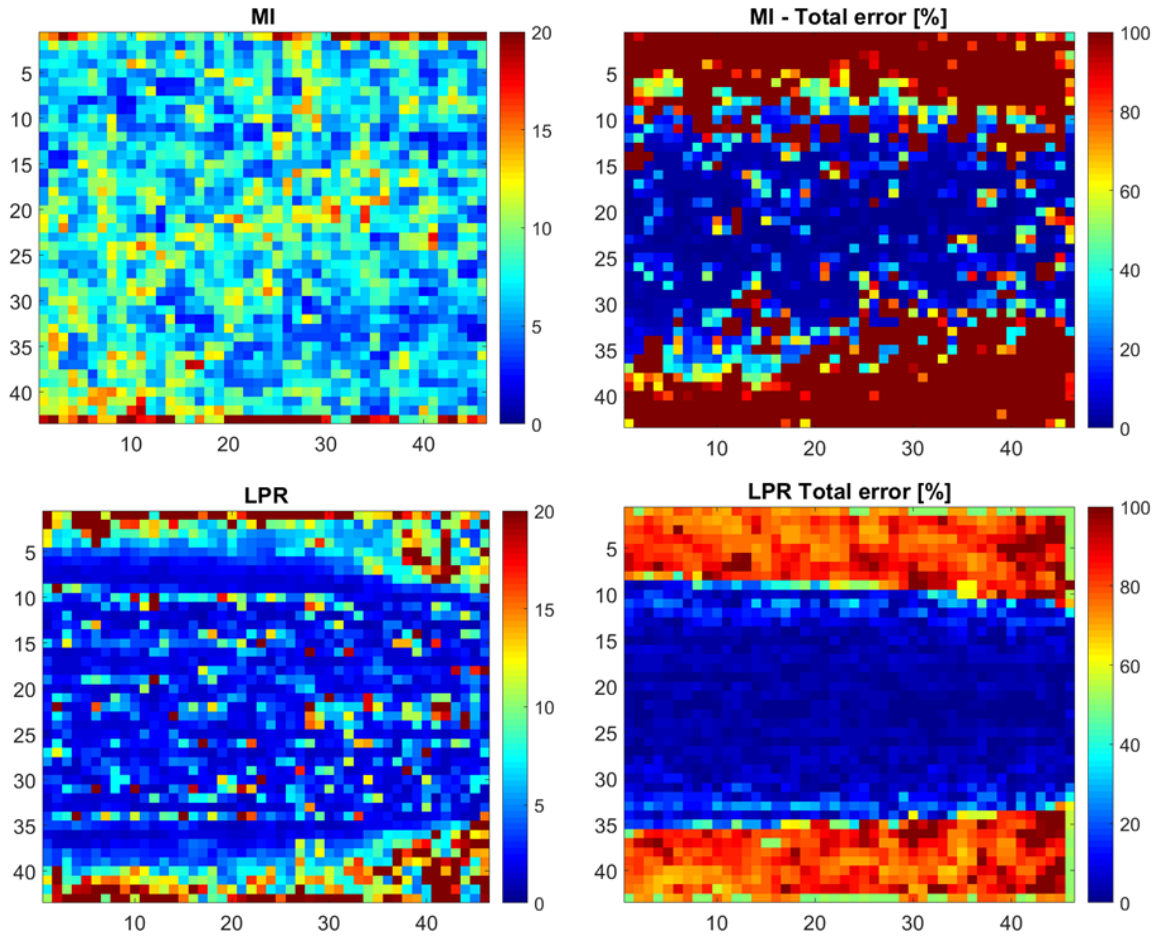

(A). Evaluated values of the MI and LPR metrics.

(B). Corresponding values of the total error depending on the size of the determined metric at each point.

FIGURE 9. Comparison of LPR and MI metrics. Calculation of the measurement error dependence according to Equations (13) and (14).

this work. In our tests, we always worked with a particles of a constant size, however, in real measurements, the diameter of the particles in the IA varies. Varying particle sizes in real data will lead to an ambiguity in determining the gradient, which significantly affects the resulting total measurement error. For this reason, in the following work, it will be necessary to perform a suitable sensitivity analysis and determine the effect of varying particle sizes within the IA. Furthermore, it will be necessary to determine the sensitivity of the procedure to other parameters in order to verify its overall uncertainty. Despite the above-mentioned ambiguities that need to be resolved in further research, we consider the procedure for determining the total error to be suitable, particularly in areas with small displacements or lower density of marking parts.

ACKNOWLEDGEMENTS

Supported by the OPST Project Green Energy Technologies Centre of UJEP, Reg. No. CZ.10.02.01/00/24_061/0000462.

REFERENCES

[1] R. D. Keane, R. J. Adrian. Optimization of particle image velocimeters. I. Double pulsed systems. *Measurement Science and Technology* **1**(11):1202, 1990. https://doi.org/10.1088/0957-0233/1/11/013

[2] K. Okamoto, S. Nishio, T. Saga, T. Kobayashi. Standard images for particle-image velocimetry. *Measurement Science and Technology* **11**(6):685, 2000. https://doi.org/10.1088/0957-0233/11/6/311

[3] J. Westerweel. *Digital particle image velocimetry: Theory and application*. Delft University Press, 1993.

[4] F. Scarano, M. L. Riethmuller. Advances in iterative multigrid PIV image processing. *Experiments in Fluids* **29**(1):S051–S060, 2000. https://doi.org/10.1007/s003480070007

[5] B. H. Timmins, B. W. Wilson, B. L. Smith, P. P. Vlachos. A method for automatic estimation of instantaneous local uncertainty in particle image velocimetry measurements. *Experiments in Fluids* **53**(4):1133–1147, 2012. https://doi.org/10.1007/s00348-012-1341-1

[6] M. Raffel, C. E. Willert, S. T. Wereley, J. Kompenhans. *Particle image velocimetry: A practical guide*. Springer Verlag, Germany, 2nd edn., 2007. https://doi.org/10.1007/978-3-540-72308-0

[7] A. Sciacchitano. Uncertainty quantification in particle image velocimetry. *Measurement Science and*

Technology **30**(9):092001, 2019. https://doi.org/10.1088/1361-6501/ab1db8

[8] A. Sciacchitano, D. R. Neal, B. L. Smith, et al. Collaborative framework for PIV uncertainty quantification: comparative assessment of methods. *Measurement Science and Technology* **26**(7):074004, 2015. https://doi.org/10.1088/0957-0233/26/7/074004

[9] A. Sciacchitano, B. Wieneke, F. Scarano. PIV uncertainty quantification by image matching. *Measurement Science and Technology* **24**(4):045302, 2013. https://doi.org/10.1088/0957-0233/24/4/045302

[10] B. Wieneke. PIV uncertainty quantification from correlation statistics. *Measurement Science and Technology* **26**(7):074002, 2015. https://doi.org/10.1088/0957-0233/26/7/074002

[11] A. Boomsma, S. Bhattacharya, D. Troolin, et al. A comparative experimental evaluation of uncertainty estimation methods for two-component PIV. *Measurement Science and Technology* **27**(9):094006, 2016. https://doi.org/10.1088/0957-0233/27/9/094006

[12] Z. Xue, J. J. Charonko, P. P. Vlachos. Signal-to-noise ratio, error and uncertainty of PIV measurement. In *International Symposium on Particle Image Velocimetry*. 2013.

[13] Z. Xue, J. J. Charonko, P. P. Vlachos. Particle image velocimetry correlation signal-to-noise ratio metrics and measurement uncertainty quantification. *Measurement Science and Technology* **25**(11):115301, 2014. https://doi.org/10.1088/0957-0233/25/11/115301

[14] Z. Xue, J. J. Charonko, P. P. Vlachos. Particle image pattern mutual information and uncertainty estimation for particle image velocimetry. *Measurement Science and Technology* **26**(7):074001, 2015. https://doi.org/10.1088/0957-0233/26/7/074001

[15] I. Tirelli, A. Ianiro, S. Discetti. A simple trick to improve the accuracy of PIV/PTV data. *Experimental Thermal and Fluid Science* **145**:110872, 2023. https://doi.org/10.1016/j.expthermflusci.2023.110872

[16] M. Maceas, A. F. Osorio, F. Bolanos. A methodology for improving both performance and measurement errors in PIV. *Flow Measurement and Instrumentation* **77**:101846, 2021. https://doi.org/10.1016/j.flowmeasinst.2020.101846

[17] S. Blahout, S. R. Reinecke, H. Kruggel-Emden, J. Hussong. On the micro-PIV accuracy and reliability utilizing non-Gaussian particle images. *Experiments in Fluids* **62**(9):191, 2021. https://doi.org/10.1007/s00348-021-03283-8

[18] J. Novotny, I. Machovska. Corrected metric for uncertainty estimation methods in particle image velocimetry. In *9^{th} World Conference on Experimental Heat Transfer, Fluid mechanics and Thermodynamics*. 2017.

[19] J. Novotny, I. Machovska. Primary peak ratio correlation to the measurement accuracy of PIV method. *Acta Polytechnica* **58**(3):189–194, 2018. https://doi.org/10.14311/AP.2018.58.0189

[20] J. Novotny, L. Novakova, I. Machovska. Advanced metric for particle image velocimetry accuracy estimation. In *19^{th} International Symposium on Applications of Laser and Imaging Techniques to Fluid Mechanics (Lisbon, Portugal)*. 2018.

[21] J. Westerweel. Fundamentals of digital particle image velocimetry. *Measurement Science and Technology* **8**(12):1379, 1997. https://doi.org/10.1088/0957-0233/8/12/002

[22] J. Westerweel. Theoretical analysis of the measurement precision in particle image velocimetry. *Experiments in Fluids* **29**(1):S003–S012, 2000. https://doi.org/10.1007/s003480070002